Efficient Simulation of Space-Time Correlated MIMO Mobile Fading Channels

Kodzovi Acolatse and Ali Abdi
Dep. of Elec. and Comp. Eng., New Jersey Institute of Technology
323 King Blvd., Newark, NJ 07102
ka2@njit.edu and ali.abdi@njit.edu

***Abstract*- Simulation of multiple-input multiple-output (MIMO) fading channels, with crosscorrelated subchannels, is of paramount importance in performance evaluation of space-time techniques in multiantenna systems. This paper focuses on four methods to simulate several spatio-temporally crosscorrelated stationary complex Gaussian processes: the spectral representation method, the sampling theorem method, the random polynomial method, and the circulant embedding method. The first three methods are based on parametric random representations, which consist of the superposition of deterministic functions with random coefficients and parameters, whereas the fourth one is built upon circulant embedding of the covariance matrix and the use of fast Fourier transform (FFT), to diagonalize a block circulant matrix . In this paper we provide a comprehensive theoretical analysis of the computational complexity of all the four methods. The performance of these techniques are also assessed, via extensive simulations, in terms of the quality of the generated samples. Our theoretical analysis and simulation results show that for MIMO channel simulations, the spectral method has much less computational complexity, with the same simulation accuracy as other methods. Matlab© files for all the four methods are available at http://web.njit.edu/~abdi.**

I. Introduction

Recent fundamental information theoretic results have shown that by exploiting antenna arrays at both the base station (BS) and mobile station (MS) and under certain conditions, unprecedented transmission rates can be achieved over wireless channels [1] [2]. Two major approaches to reach such high capacities are space-time coding [3] and V-BLAST architecture [4], which have driven the recent surge of numerous research and development activities for very high speed transmission systems. In general, multiantenna systems attempt to use both time- and space-domain channel characteristics, via appropriate coding and detection schemes. Needless to say, software simulation of multiple-input multiple-output (MIMO) channels is essential for evaluating the performance of different multiantenna space-time coding/processing techniques, before expensive hardware experiments.

A useful MIMO simulator should be able to generate multiple crosscorrelated processes. There are few papers, which address this issue for receive-only diversity schemes (see [5] and references therein). To the best of our knowledge, only in [5] the simulation of MIMO channels is addressed properly (for the limitations of other techniques, see [5]). However, only the vector autoregressive (AR) simulation approach is discussed in [5], whereas there are other techniques that could serve as efficient candidates for MIMO simulation. In this paper we focus on four methods for simulating a vector of correlated complex Gaussian processes. We also provide a comprehensive theoretical analysis of the computational complexity of all the four methods, not considered in the past.

For computer implementation of these methods, one needs either the crosscorrelations or the crossspectra among the processes of different subchannels. Here we use a recently proposed space-time macrocell model [6], which provides closed-form expressions for correlations and spectra of interest, and includes many key physical channel parameters in compact forms. This model is also used in the MIMO simulation study of [5]. One can use the micro and picocell model of [7] as well.

The rest of this paper is organized as follows. In Sections II, III, IV and V, four simulation techniques are discussed in detail. To demonstrate the accuracy of the algorithm, theoretical and average simulation results for the level crossing rate (LCR), different types of correlation functions, and the probability density function (PDF) are compared. Section VI is devoted to the extensive comparison of the computational complexity of the algorithms. Concluding remarks are presented in Section VII.

II. Spectral Representation Method

The first method employs the spectral representation model. This model works according to the spectral representation theorem which states that a weakly stationary process can be viewed as a superposition of harmonics with random amplitudes and phases [8] [9]. Specifically, it is based on the discretization of the frequency band of the process and the representation of the process by a sum of complex exponentials. The probabilistic characteristics of the generated samples functions converge to that of the target process, as the number of terms in the exponential series increases.

Spectral Representation Theorem: Let $\{Y(t), t>0\}$ be a wide sense stationary vector process with *m* complex-valued components of zero mean and covariance functions

$$C_{kl}(\tau) = E[Y_k(t)Y_l^*(t+\tau)], \quad k,l = 1,...,m, \tag{1}$$

and the associated spectral densities

$$S_{kl}(f) = \int_{-\infty}^{\infty} e^{-i2\pi f\tau} C_{kl}(\tau) d\tau, \tag{2}$$

where $i=\sqrt{-1}$ and $k,l = 1,2,...,m$. Then there exists a unique process $Z(f)$ [9] such that

$$Y(t) = \int_{-\infty}^{\infty} e^{i2\pi f t} dZ(f), \tag{3}$$

where $dZ(f)$ is a vector of m complex-valued processes with mean zero and the following covariance function [10]

$$E[dZ_k(f)dZ_l^*(\xi)] = S_{kl}(f)df, \quad f=\xi, \\ = 0, \quad \text{otherwise.} \tag{4}$$

where f and ξ are frequency variables.□

If the vector process $Z(f)$ is Gaussian, $Y(t)$ delivered by the spectral representation formula is also a Gaussian process [11]. $Y(t)$ is assumed to be band-limited in the frequency interval $(-f_{\max}, f_{\max})$. However, if the process has power over the entire frequency range, one can select a cutoff frequency $f_{\max} < \infty$ such that for all *k* and *l*

$$\int_{-\infty}^{\infty} S_{kl}(f)df \approx \int_{-f_{\max}}^{f_{\max}} S_{kl}(f)df \ . \qquad (5)$$

To obtain the discrete version of (3), let us divide the frequency band $(-f_{\max}, f_{\max})$ into q nonoverlapping intervals (α_{r-1}, α_r), $r = 1, 2, ..., q$, with length $df_r = \alpha_r - \alpha_{r-1} = 2f_{\max}/q$. A discrete approximation of order q of Eq. (3) is given by the following expression [11]

$$\hat{Y}^{(q)}(t) = \sum_{r=1}^{q} A_r e^{i2\pi f_r t} \qquad (6)$$

where A_r is a zero mean Gaussian vector with covariance

$$E[A_{r,k} A_{p,l}^*] = \int_{\alpha_{r-1}}^{\alpha_r} S_{kl}(f)df \approx S_{kl}(f_r)df_r, \ \text{if} \ r = p,$$
$$= 0, \ \text{if} \ r \neq p,$$

$r, p = 1, ..., q$, such that f_r is the midpoint of the interval (α_{r-1}, α_r), and df_r is the length of the interval (α_{r-1}, α_r).

It is shown in [11] that the probabilistic characteristics of $\hat{Y}^{(q)}(t)$ approach those of $Y(t)$ as $q \to \infty$. So, Eq. (6) can be used as a good approximation of $Y(t)$ if q is sufficiently large. Note that the process in (6) is periodic with period $q/f_{\max}$, as mentioned in [12]. So, to generate the process in $[0, T]$, one should choose q large enough such that $T < q/f_{\max}$.

The simulation of the vector process $\hat{Y}^{(q)}(t)$ involves two steps

1- Generation of samples of the complex Gaussian vector A_r (the Cholesky factorization-based algorithm of [11], Section 4.2, is used in this paper).

2- Realization of the process using Eq. (6) in which A_r is replaced by its samples generated in the first step.

Simulation: To simulate a 2×2 MIMO channel using this method, we use the MIMO correlation model given in Eq. (12) of [6] for the autocorrelations and crosscorrelations of four subchannels $h_{11}(t)$, $h_{12}(t)$, $h_{21}(t)$, and $h_{22}(t)$

$$C_{h_{ip}h_{mq}}(\tau) = [I_0(\kappa)]^{-1} \exp[ic_{pq}\cos(\alpha_{pq})] \times$$
$$I_0(\{\kappa^2 - a^2 - b_{lm}^2 - c_{pq}^2\Delta^2\sin^2(\alpha_{pq}) +$$
$$2ab_{lm}\cos(\beta_{lm} - \gamma) + 2c_{pq}\Delta\sin(\alpha_{pq})[a\sin(\gamma) - b_{lm}\sin(\beta_{lm})] -$$
$$i2\kappa[a\cos(\mu - \gamma) - b_{lm}\cos(\mu - \beta_{lm}) - c_{pq}\Delta\sin(\alpha_{pq})\sin(\mu)]\}^{1/2}), \qquad (7)$$

where $I_0(.)$ is the zero order modified Bessel function, $a = 2\pi f_m \tau$, $b_{lm} = 2\pi d_{lm}/\lambda$, $c_{pq} = 2\pi\delta_{pq}/\lambda$, f_m is the maximum Doppler shift, d_{lm} denotes the antenna spacing at the MS, δ_{pq} is the antenna spacing at the BS, λ is the wavelength, 2Δ is the maximum angle spread at the BS, μ accounts for the mean angle of arrival (AOA) seen by the MS, κ controls the width of AOA at the MS, α_{pq} and β_{lm} are the angles which specify the orientations of the BS and MS arrays, respectively, and finally γ is the direction of the motion of MS. Note that $l, m, p, q = 1, 2$.[1] All these parameters are clearly depicted in Fig. 1 of [6]. The corresponding power spectrum can be shown to be

$$S_{h_{ip}h_{mq}}(f) = \exp[ic_{pq}\cos(\alpha_{pq})] \Big/ [I_0(\kappa)\pi\sqrt{f_m^2 - f^2}]$$
$$\times \exp\{-[\kappa\cos(\gamma - \mu) + i\vartheta_1](f/f_m)\}$$
$$\times \cosh\{[\kappa\sin(\gamma - \mu) + i\vartheta_2]\sqrt{1 - (f/f_m)^2}\}, \quad |f| \le f_m,$$

where cosh(.) is the hyperbolic cosine and

$$\vartheta_1 = b_{lm}\cos(\beta_{lm})\cos(\gamma) + [c_{pq}\Delta\sin(\alpha_{pq}) + b_{lm}\sin(\beta_{lm})]\sin(\gamma),$$
$$\vartheta_2 = b_{lm}\cos(\beta_{lm})\sin(\gamma) - [c_{pq}\Delta\sin(\alpha_{pq}) + b_{lm}\sin(\beta_{lm})]\cos(\gamma).$$

For the parameters, we choose the same values used in [5], i.e., $f_m = 0.05$ Hz, $d_{12}/\lambda = 0.5$, $\delta_{12}/\lambda = 17$, $\kappa = 0$ (isotropic scattering), $\Delta = 4^\circ$, $\alpha_{12} = \beta_{12} = 90^\circ$ (parallel arrays), and $\gamma = 180^\circ$. For the number of nonoverlapping frequency bins we have chosen $q = 60$, which gives a reasonable match between the simulated and theoretical correlations. With other parameters fixed, normally the quality of simulation improves as q increases. We have generated 100 MIMO channel realizations, each realization consists of four N-sample complex Gaussian time series, $N = 1000$. The simulated LCR of the envelope of $h_{11}(t)$, and the autocorrelations, crosscorrelations, and histograms of the real parts (inphase components), averaged over 100 realizations, are plotted in Fig. 1, Fig. 2, Fig. 3, and Fig. 4, respectively, along with the theoretical curves. For the theoretical LCR of $|h_{11}(t)|$ we have used [13]

$$N_R = \sqrt{\pi} f_m \frac{R}{\sigma} e^{-\frac{1}{2}\left(\frac{R}{\sigma}\right)^2},$$

where R is the level and σ^2 is the variance of each inphase and quadrature components. In the simulations we have $\sigma^2 = 1$.

In this method, the size of the covariance matrix that needs Cholesky factorization is $n_{BS}n_{MS} \times n_{BS}n_{MS}$, where n_{BS} and n_{MS} are the number of BS and MS antenna elements, respectively. In our particular example, the size is 4×4 as $n_{BS} = n_{MS} = 2$. Note that the total number of required Cholesky factorizations is q, which is 60 in our example.

III. Sampling Theorem Method

The second method is based on the sampling theorem for random processes and its generalization to vector processes. It simply states that a band limited process consists of a superposition of deterministic functions of time with random amplitudes. Consider a deterministic function $\theta(.)$ such that its Fourier transform is zero outside a bounded frequency range $(-f_{\max}, f_{\max})$, $f_{\max} < \infty$. According to the sampling theorem [14]

$$\theta(t) = \sum_{u=-\infty}^{\infty} \theta(t_0 + uT) a_u(t - t_0), \qquad (8)$$

in which

$$a_u(t) = \sin[\pi(t - uT)/T] / [\pi(t - uT)/T], \qquad (9)$$

where $T = 1/(2f_{\max})$ and t_0 are real numbers. Let $Y(t)$ be a zero-mean stationary vector process with m complex-valued components defined over the frequency band $(-f_{\max}, f_{\max})$, with correlation function $C_{kl}(\tau) = E[Y_k(t)Y_l^*(t + \tau)]$, where $k, l = 1, 2, ..., m$. A parametric representation of the process $Y(t)$ is given in [15]

$$\hat{Y}_k^{(n)}(t) = \sum_{u=n_t-n}^{n_t+n+1} \hat{Y}_k^{(u)} a_u(t), \quad n_t T \le t \le (n_t + 1)T, \qquad (10)$$

in which $n_t = [t/T]$ denotes the largest integer smaller than t/T, $[(n_t - n)T, (n_t + n + 1)T]$ represents a window where the positive integer n determines the size of the window, and $\hat{Y}_k^{(u)} = Y_k(uT)$ are values of the k-th component of the vector process $Y(t)$ at equally-spaced time instants, referred to as nodal points. Note that for each value of t, there is a fixed number of nodal points, which is $2(n+1)$ according to (10).

It is shown in [15] that $\hat{Y}^{(n)}(t)$ has the same covariance function as $Y(t)$, as $n \to \infty$. Therefore, $\hat{Y}^{(n)}(t)$ can be used as a good approximation of $Y(t)$, if n is large enough.

---

[1] Obviously the indices l, m, p, and q in (7) are different from the previously-defined parameters such as the number of complex processes m in the spectral representation theorem, the number of frequency intervals q in (6), and so on.

The simulation procedure described in [15] is as follows. Let $t \in [n_t T, (n_t+1)T]$. The process $\hat{Y}_k^{(n)}(t)$ in (10) depends on the nodal values $\{Y_k((n_t-n)T), ..., Y_k((n_t+n+1)T)\}$. A realization of the process $\hat{Y}_k^{(n)}(t)$ can be obtained for $t \in [n_t T, (n_t+1)T]$ using theses nodal values according to (10). To generate the samples for the interval $t \in [(n_t+1)T, (n_t+2)T]$, we need to generate the single sample $Y_k((n_t+n+2)T)$ first and then use Eq. (10). The single sample $Y_k((n_t+n+2)T)$ depends on all the previously generated values of $\hat{Y}_k^{(n)}(t)$ at the nodal points. For simplicity, this dependence can be reduced to the past $2(n+1)$ nodal values [11].

In summary the major steps of this algorithm are

1- Samples of the vector process $Y(t)$ at the nodal points need to be generated (the Cholesky factorization-based algorithm of [11], Section 4.2, is used in this paper).

2- A realization of $Y(t)$ now can be constructed using (10), along with increasing *t*, starting from $t \in [0, T]$.

Simulation: The sampling method is used to simulate the 2×2 MIMO Rayleigh fading channel of Section II and the same simulation results as those shown in Fig. 1 - Fig. 4 are obtained. The parameter n is set to 30, as it exhibits a good match between the simulated and theoretical correlations. With other parameters fixed, normally the quality of simulation improves as *n* increases.

The size of the covariance matrix that needs Cholesky factorization is $(2n+3)n_{BS}n_{MS} \times (2n+3)n_{BS}n_{MS}$, which in our example reduces to $(60+3)4 \times (60+3)4 = 252 \times 252$. Note that the Cholesky factorization should be carried out only once.

IV. Random Polynomial Method

The third method is the random polynomial method that is based on the parametric representation of the process of interest in terms of interpolation polynomials and spline functions.

Let $\{Y(t), t \in [a,b]\}$ be a vector process with *m* complex components. The approximation of the *k*-th component of $Y(t)$ based on linear spline functions is given by

$$\hat{Y}_k^{(p)}(t) = [1-\xi(t)]\hat{Y}_k^{(p_t)} + \xi(t)\hat{Y}_k^{(p_t+1)}, \qquad (11)$$

for $t \in [a + p_t T, a + (p_t+1)T]$, where p_t is the largest integer smaller than $(t-a)/T$, $\xi(t) = (t - a - p_t T)/T$, $T = (b-a)/p$, p is the number of time subintervals, and finally $\hat{Y}_k^{(p)}(t)$'s are values of the *k*-th component of $Y(t)$ at time instants $t = a + lT$, $l = 0, 1, ..., p$, referred to as nodal points.

It is shown in [11] that the covariance function of $\hat{Y}^{(p)}(t)$ approaches the covariance function of $Y(t)$, as $p \to \infty$. Hence, $\hat{Y}^{(p)}(t)$ serves as a good approximation for large *p*.

This simulation technique involves two steps

1- Samples of the vector process consisting of the values of $Y(t)$ at the nodal points need to be generated (the Cholesky factorization-based algorithm of [11], Section 4.2, is used in this paper).

2- A realization of $Y(t)$ should be calculated using (11).

Simulation: The random polynomial method is used to simulate the 2×2 MIMO Rayleigh fading channel of Section II, and the simulation results are exactly the same as Fig. 1 - Fig. 4. The parameter *p* is set to 60 since it provides a good match between the simulated and theoretical correlations. With other parameters fixed, normally the quality of simulation improves as *p* increases.

The size of the covariance matrix that needs Cholesky factorization is $(p+1)n_{BS}n_{MS} \times (p+1)n_{BS}n_{MS}$, which is equal to $(60+1)4 \times (60+1)4 = 244 \times 244$ in our example. Note that there is only one Cholesky factorization, similar to the sampling method.

V. Circulant Embedding Method

This approach is based on the observation that any (block) Toeplitz matrix can be embedded in a (block) circulant matrix [16]. The two main components of this method are: (i) circulant embedding of the block Toeplitz covariance matrix, and (ii) the use of the fast Fourier transform (FFT), to diagonalize the block circulant matrix. In what follows, we provide a summary of [16].

Let $\{Y(t), t > 0\}$ be a wide sense stationary vector process composed of *m* complex-valued components with zero mean and the covariance functions defined in (1). We want to generate *N* samples of $Y(t)$ at $t = 0, T_s, ..., (N-1)T_s$, over the interval $[0, T]$. Obviously $T_s = T/(N-1)$. Let us define the $m \times m$ covariance matrix $\bar{C}(j)$ such that its (*k*,*l*)-th element is given by $C_{kl}(jT_s)$, $j = 0, 1, ..., N-1$, with $C_{kl}(.)$ defined in (1). Then we construct the $Nm \times Nm$ block Toeplitz covariance matrix *C*, with block elements given by $\bar{C}(j)$s. Obviously the first row of *C* is given by $[\bar{C}(0)\bar{C}(1)...\bar{C}(N-1)]$. The vector process $Y(t)$ can be generated by embedding its block Toeplitz covariance matrix C into an $mr \times mr$ circulant matrix G, where *r* determines the size of the embedding matrix *G*. Note that *r* should be chosen such that $r \geq 2(N-1)$ and *G* is nonnegative definite. Choosing *r* as a power of 2 can increase the efficiency of this method. If *G* is negative definite, we have to increase *r* until *G* is nonnegative definite. If one cannot find *r* such that *G* is nonnegative definite or if *r* is too large to be practical, the approximation described in [17] may be used.

We construct *G* according to $G = \text{circ}([g(0)\, g(1) ... g(r-1)])$, where each $g(.)$ is an $m \times m$ matrix and circ(.) cyclically shifts its (block row) argument from left to right, to build *G*. Note that $g(.)$s should be chosen such that G is a Hermitian matrix with nested block circulant structure and C is a submatrix of G. These $g(.)$ matrices should be constructed as follows

$$g(l) = \begin{cases} \bar{C}(l), & 0 \leq l \leq r/2, \\ \bar{C}(r-l), & r/2 < l \leq r-1, \end{cases} \qquad (12)$$

Based on the construction in (12), each $Nm \times Nm$ submatrix of G, down the diagonal, is equal to C. Therefore, if G is nonnegative definite, it can be considered as the covariance matrix of a stationary vector process $X(t)$, sampled at the rate of $1/T_s$. Furthermore, any *N* consecutive elements of $X(t)$ form a realization of $Y(t)$.

It is important to note that the circulant matrix *G* can be decomposed as

$$G = (Q \otimes I)\text{diag}(\{A(0), A(1), ..., A(r-1)\})(Q^H \otimes I),$$

where *Q* is an $r \times r$ unitary matrix with the (*k*,*l*)-th element given by $Q_{kl} = r^{-1/2}\exp(-i2\pi kl/r)$, $k, l = 0, 1, ..., r-1$, $\otimes$ denotes the Kronecker product of two matrices, *I* is an $m \times m$ identity matrix, diag(.) constructs a (block) diagonal matrix of its arguments, ^{H} is transpose conjugate, and each $m \times m$ Hermitian matrix $A(l)$, $0 \leq l \leq r-1$, is defined as

$$A(l) = \sum_{j=0}^{r-1} g(j)\exp(-i2\pi jl/r).$$

Upon eigen decomposition we get $A(l) = R(l)\Lambda(l)R(l)^H$, where $R(l)$ is an $m \times m$ unitary matrix and $\Lambda(l)$ is a diagonal matrix with eigenvalues of $A(l)$ on its diagonal. Each $A(l)$ has real eigenvalues $\zeta_1(l), ..., \zeta_m(l)$ and it follows that G is nonnegative definite if and only if

$$\zeta_j(l) \geq 0, \quad 1 \leq j \leq m \text{ and } 0 \leq l \leq r-1. \qquad (13)$$

If (13) holds, then we have

$$G^{1/2} = (Q \otimes I)\text{diag}(\{A(0)^{1/2}, A(1)^{1/2}, ..., A(r-1)^{1/2}\})(Q^H \otimes I),$$

as the unique nonnegative definite square root of G. Consequently, T_s – spaced samples of the vector process $X(t)$, i.e., $X(0), X(T_s), ..., X((r-1)T_s)$, can be simulated via $G^{1/2}W$, where W is an $mr \times 1$ vector of independent standard Gaussian random numbers. Any N consecutives elements of theses r samples, e.g., $X(0), X(1), ..., X(N-1)$, is a realization of the process $Y(t)$.

The simulation algorithm of the circulant embedding method can be summarized as follows

1- Compute the first block row of G (m rows), using (12).
2- Compute $A(l)$, $0 \le l \le r-1$, with $m(m+1)/2$ applications of FFT (FFT of the first block row of G).
3- Compute $R(l)$ and $\Lambda(l)$ such that $A(l) = R(l)\Lambda(l)R(l)^H$.
4- Simulate $(Q^H \otimes I)W$ directly, as described in [16], where W is an $mr \times 1$ vector of independent standard Gaussian random numbers.
5- Let $a(l) = A(l)^{1/2}(Q^H \otimes I)W = R(l)\Lambda(l)^{1/2}R(l)^H(Q^H \otimes I)W$.
6- Compute T_s – spaced samples of $X(t)$ with m applications of FFT, i.e., FFT of $a(l)$, since $(Q \otimes I)a(l)$ is the FFT of $a(l)$.
7- Take N consecutive samples of $X(t)$, to get a realization of $Y(t)$.

Note that in addition to $r \ge 2(N-1)$ such that G is nonnegative definite, r should be chosen such that $r = 2^k$ or 3^k, for some positive integer k, to make the FFT calculation fast.

The circulant structure of matrix G is the key to the speed and efficiency of this method. All the relevant calculations can be performed using FFT.

Simulation: The circulant embedding method is used to simulate the 2×2 MIMO Rayleigh fading channel of Section II and the simulations are the same as those presented in Fig. 1 - Fig. 4. For $N = 1000$, we have chosen $r = 2^{11} = 2048$, to get a good match between simulated and theoretical correlations.

In this method, the size of the matrix that needs eigen decomposition is $n_{BS}n_{MS} \times n_{BS}n_{MS}$, which in our example is 4×4. Note that the total number of required Eigen decompositions is r, which is 2048 in our example.

VI. Computational Complexity

As all the figures show, with proper selection of the control parameters, very close agreement between a variety of theoretical and simulated characteristics of a vector complex Gaussian process, such as LCR, correlations, and histograms, can be obtained. So, computational complexity is the major factor in choosing between these four methods. After careful examination of all the operations, which have to be carried out in each method, in Table I we provide a summary of the computational complexity of different steps in each method.

In Table I, $O(.)$ stands for the order, whereas the number of operations shows the number of multiplications plus divisions (to simplify the analysis, we consider real and complex operations the same). Note that Eqs. (6), (10), and (11) represent the main expression for the spectral, sampling, and polynomial methods, respectively, whereas steps 2 and 5 in the embedding method constitute the main expressions.

As an example, the number of operations in all the four methods are given in Table II, for our 2×2 simulation, where $n_{MS} = n_{BS} = 2$, $q = 60$, $n = 30$, $p = 60$, and $N = 1000$, therefore $r = 2^{11} = 2048$. Clearly, spectral method is much superior to the others. It is specially efficient when it comes to matrix decomposition.

VII. Conclusion

Due to the high spectral efficiency of multiantenna systems, development of space-time coding/detection schemes has received a great deal of attention in recent years. In this paper, the utility of four different methods, i.e., spectral, sampling, polynomial, and embedding are studied, for generating realizations of crosscorrelated complex-valued Gaussian processes. Based on extensive Monte Carlo simulations, it has been observed that with proper choices of parameters, all the methods provide very accurate realizations in terms of the level crossing rate, correlations, and histograms. However, our theoretical complexity analysis has revealed that the spectral method requires much lower computational effort, hence, more suitable for simulation of MIMO fading channels. Matlab© files of all the four methods can be obtained from http://web.njit.edu/~abdi.

TABLE I

COMPARISON OF THE COMPUTATIONAL COMPLEXITY

	Spectral	Sampling	Polynomial	Embedding
Covariance matrix calculation	Size: $n_{MS}n_{BS}$, #operations: $50(n_{MS}n_{BS})^2 q$	Size: $n_{MS}n_{BS}(2n+3)$, #operations: $60[n_{BS}n_{MS}(2n+3)]^2$	Size: $n_{BS}n_{MS}(p+1)$, #operations: $60[n_{MS}n_{BS}(p+1)]^2$	Size: $n_{MS}n_{BS}r$, #operations: $60(n_{BS}n_{MS})^2 \frac{r}{2}$
Cholesky or eigen decomposition	q times, #operations: $O(qn_{MS}^3 n_{BS}^3)$	1 time, #operations: $O([n_{MS}n_{BS}(2n+3)]^3)$	1 time, #operations: $O([n_{MS}n_{BS}(p+1)]^3)$	r times, #operations: $O(rn_{MS}^3 n_{BS}^3)$
Generating independent white vectors	q times, Size: $n_{MS}n_{BS}$	1 time, Size: $n_{MS}n_{BS}(2n+2)$ and N times, Size: $n_{MS}n_{BS}$	1 time, Size: $n_{MS}n_{BS}(p+1)$	1 time, Size: $n_{MS}n_{BS}r$
Coloring the white vectors	#operations: $(n_{MS}n_{BS})^2 q$	#operations: $[n_{MS}n_{BS}(2n+2)]^2 + N(n_{MS}n_{BS})^2$	#operations: $[n_{MS}n_{BS}(p+1)]^2$	#operations: $(n_{MS}n_{BS})^2 r$
Calculating the main expression	#operations: $n_{MS}n_{BS}qN + 2qN$	#operations: $4(2n+3)N$	#operations: $10N$	#operations: $n_{MS}n_{BS}/2 \times (n_{MS}n_{BS}+3) \times r\log_2 r$

TABLE II

NUMERICAL VALUES OF THE COMPUTATIONAL COMPLEXITY

	Spectral	Sampling	Polynomial	Embedding
Covariance ...	48,000	3,810,240	3,572,160	983,040
Cholesky …	O(3,840)	O(16,003,008)	O(14,526,784)	O(131,072)
Generating …	240	4488	244	8192
Coloring …	960	77,504	59,536	32,768
Calculating ...	360,000	252,000	10,000	315,392

REFERENCES

[1] G. J. Foschini and M. J. Gans, "On limits of wireless communications in a fading environment when using multiple antennas," *Wireless Pers. Commun.*, vol. 6, pp. 311-335, 1998.

[2] I. E. Telatar, "Capacity of multi-antenna Gaussian channels," *European Trans. Telecommun. Related Technol.*, vol. 10, pp. 585-595, 1999.

[3] V. Tarokh, N. Seshadri, and A. R. Calderbank, "Space-time codes for high data rate wireless communication: Performance criterion and code construction," *IEEE Trans. Inform. Theory*, vol. 44, pp. 744-765, 1998.

[4] G. D. Golden, C. J. Foschini, R. A. Valenzuela, and P. W. Wolniansky, "Detection algorithm and initial laboratory results using V-BLAST space-time communication architecture," *Electron. Lett.*, vol. 35, pp. 14-16, 1999.

[5] K. E. Baddour and N. C. Beaulieu, "Accurate simulation of multiple cross-correlated fading channels," in *Proc. IEEE Int. Conf. Commun.*, New York, 2002, pp. 267-271.

[6] A. Abdi and M. Kaveh, "A space-time correlation model for multielement antenna systems in mobile fading channels," *IEEE J. Select. Areas Commun.*, vol. 20, pp. 550-560, 2002.

[7] K. Raghukumar, "Spatio-temporal correlation models for indoor MIMO channels," M.S. Thesis, Dept. of Elec. and Comp. Eng., New Jersey Institute of Technology, Newark, NJ, 2003.

[8] A. M. Yaglom, *Correlation Theory of Stationary and Related Random Functions I: Basic Results*. New York: Springer, 1987.

[9] H. Cramer and M. R. Leadbetter, *Stationary and Related Stochastic Processes: Sample Function Properties and Their Applications*. New York: Wiley, 1967.

[10] A. Gutjahr, S. Hatch, B. Bullard, and L. Hughson, "Conditional simulation and contaminant flow modeling: Effects of linearization," New Mexico Waste-Management Education and Research Consortium & U.S. Dept. of Energy, Tech. Rep. WERC-91-08, 1993.

[11] M. Grigoriu, *Applied non-Gaussian Processes: Examples, Theory, Simulation, Linear Random Vibration, and MATLAB Solutions*. Englewood Cliffs, NJ: Prentice-Hall PTR, 1995.

[12] M. Shinozuka and G. Deodatis, "Simulation of stochastic processes by spectral representation," *Appl. Mech. Rev.*, vol. 44, pp. 191-203, 1991.

[13] R. Janaswamy, *Radiowave Propagation and Smart Antennas for Wireless Communications*. Boston, MA: Kluwer, 2001.

[14] E. Wong and B. Hajek, *Stochastic Processes in Engineering Systems*. New York: Springer, 1985.

[15] M. Grigoriu, "Simulation of stationary processes via a sampling theorem," *J. Sound Vib.*, vol. 166, pp. 301-313, 1993.

[16] G. Chan and A. T. A. Wood, "Simulation of stationary Gaussian vector fields," *Stat. Comp.*, vol. 9, pp. 265-268, 1999.

[17] A. T. A. Wood and G. Chan, "Simulation of stationary Gaussian processes in $[0,1]^d$," *J. Comput. Graph. Stat.*, vol. 3, pp. 409-432, 1994.

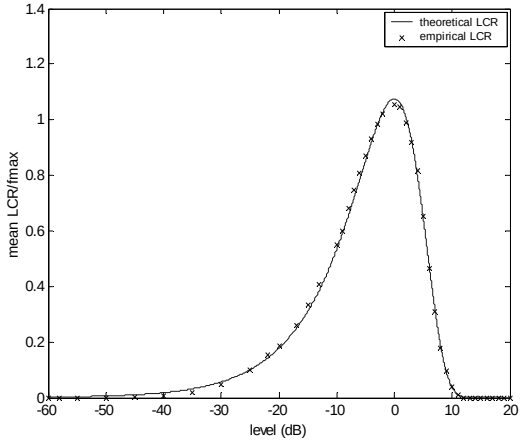

Fig. 1. Simulated and theoretical level crossing rates of the envelope of the first subchannel, $|h_{11}(t)|$, for the spectral method, as a function of $20\log_{10}(R/\sigma)$.

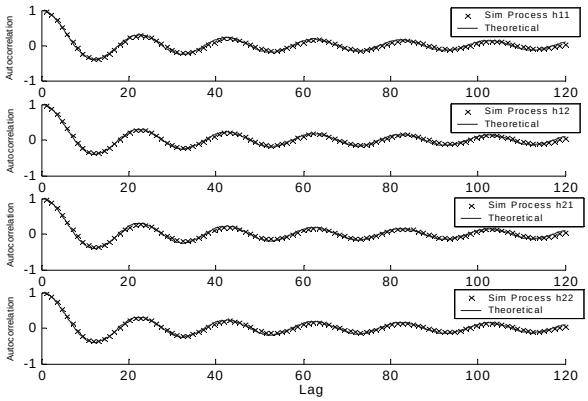

Fig. 2. Simulated and theoretical autocorrelations for the spectral method.

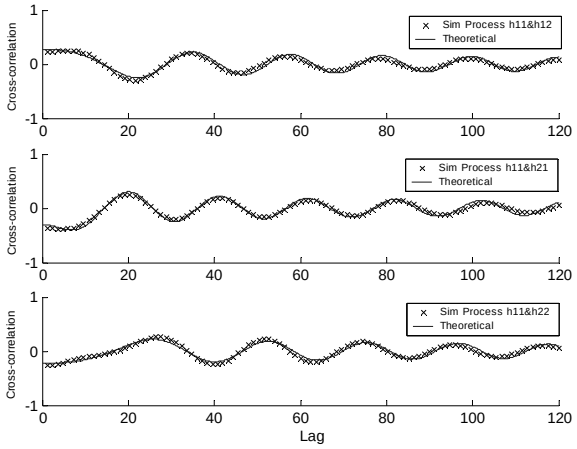

Fig. 3. Simulated and theoretical crosscorrelations for the spectral method.

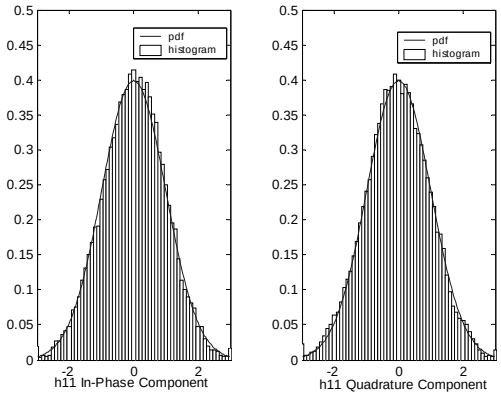

Fig. 4. Simulated and theoretical distributions for the spectral method.